

Data Driven Density Functional Theory: A case for Physics Informed Learning

Peter Yatsyshin^{a,1}, Serafim Kalliadasis^b, and Andrew B. Duncan^{a,c}

^aThe Alan Turing Institute; ^bDepartment of Chemical Engineering, Imperial College London; ^cDepartment of Mathematics, Imperial College London

This manuscript was compiled on June 28, 2022

We propose a novel data-driven approach to solving a classical statistical mechanics problem: given data on collective motion of particles, characterise the set of free energies associated with the system of particles. We demonstrate empirically that the particle data contains all the information necessary to infer a free energy. While traditional physical modelling seeks to construct analytically tractable approximations, the proposed approach leverages modern Bayesian computational capabilities to accomplish this in a purely data-driven fashion. The Bayesian paradigm permits us to combine underpinning physical principles with simulation data to obtain uncertainty-quantified predictions of the free energy, in the form of a probability distribution over the family of free energies consistent with the observed particle data. In the present work we focus on classical statistical mechanical systems with excluded volume interactions. Using standard coarse-graining methods, our results can be made applicable to systems with realistic attractive-repulsive interactions. We validate our method on a paradigmatic and computationally cheap case of a one-dimensional fluid. With the appropriate particle data, it is possible to learn canonical and grand-canonical representations of the underlying physical system. Extensions to higher-dimensional systems are conceptually straightforward.

Bayesian statistics | Free energy functional

Statistical mechanics relates macroscopic properties of matter, such as pressure, magnetisation or electric charge, to its underlying microscopic structure, given by the interactions between the constituent atomic particles. This is accomplished by casting the desired macroscopic quantities as averages over particle positions and velocities. Since in equilibrium particle velocities follow the Maxwell distribution, the central problem of equilibrium statistical mechanics is in representing the distribution over particle positions. Due to correlations between the particles, this is a highly non-trivial task, even for systems with simple interparticle interactions. Direct application of first-principles and the Liouville theorem leads to a hierarchy of correlation functions and requires a closure assumption to be computationally tractable.

An alternative approach, known as Density Functional Theory (DFT) seeks to develop good approximations for the free energy, exploiting the property that the free energy is a functional of the one-body density function $\rho(\mathbf{r})$, which characterises the probability of finding a particle at position \mathbf{r} , and that the equilibrium distribution is the one that minimizes the free energy (1). Modern DFT has a versatile plethora of computationally efficient approximate methods. In quantum DFT, these encompass effective approximations for the exchange-correlation energy of the electronic density, and in classical DFT, these constitute a library of methods to approximate the excess-over-ideal Helmholtz free energy $F[\rho]$, to account for interactions in classical many-body systems. In the present work we focus on classical DFT and develop a data-driven approach to the derivation of a free energy functional of systems with excluded volume interactions based on simulation data.

Classical DFT is widely used in soft matter, liquid state theory and biology. A popular method for constructing highly accurate approximate expressions for $F[\rho]$ is based on coarse-graining complex intermolecular interactions. This approach can also be viewed as the extension of the Born-Oppenheimer approximation to classical systems, whereby intermolecular effects happening on different spatiotemporal scales are decoupled and accounted for separately. Coarse-grained DFTs are successfully used in studies of phase transitions, interfacial phenomena, colloidal and polymer fluids, surfactants, liquid crystals, crystalline solids and glasses (2). The key ingredient of a coarse-grained DFT is an appropriately chosen reference system, which adequately

Significance Statement

For the first time a physics-informed Bayesian inference framework is proposed, which yields a humanly interpretable description of a many-body system with complex interactions in terms of a distribution over possible Helmholtz free energy functionals. This distributional model allows for uncertainty quantification and model ranking. The only required input to obtain the analytically tractable free energy is small amounts of particle simulation data. Present work offers a first step towards equation-free, inferential modelling of many-body systems, where small-scale simulations are used to automatically capture essential patterns of the collective behaviour, yielding a description that can be scaled to system sizes beyond the simulation capabilities.

The authors declare no conflict of interest.

All authors contributed equally.

¹ To whom correspondence should be addressed. E-mail: pyatsyshin@turing.ac.uk

captures the important inter-particle correlations. For example, in a Lennard-Jones fluid the intermolecular interactions can be decoupled into *sharp short-range repulsions*, caused by the overlap of the electron orbitals and the Pauli exclusion principle, and *weak long-range attractions*, which are due to the dipole-dipole electromagnetic attractions. A highly accurate coarse-grained $F[\rho]$ is given by that of a hard sphere fluid, plus a mean-field attractive term, which acts as a perturbation. It turns out that many fluids of interest can be adequately described by similar coarse-graining techniques, i.e. by stacking hierarchies of reference systems with hard-core constituent particles of different shapes and sizes, and adding the mean-field attractions perturbatively (2). Thus, developing reliable approximations for the Helmholtz free energy of fluids, made up of hard particles is of central importance to the DFT modelling of realistic systems.

1. Statistical model of a hard-body free energy functional

Unfortunately, exact $F[\rho]$ is known for only a very special case of a one-dimensional (1D) fluid of hard rods (HR), constrained to a line (3). Approximate DFTs were developed for a handful of relatively simple systems, such as hard spheres or parallel hard cubes (4). The aim of the present work is to introduce, for the first time, the Bayesian paradigm, which provides a principled framework for learning $F_{ex}[\rho]$ in a hard-particle fluid based on observations of the particle trajectories. Since our goal is methodological, we showcase our inference method in application to the simplest possible system: 1D HR on a line. This system is chosen for two reasons. Firstly, access to exact $\rho(\mathbf{r})$ allows us to easily benchmark the inference scheme against the truth. Secondly, data generation is easy in 1D, which facilitates convergence studies and comparison to a brute-force statistical inference approach. Application of our principled approach to more complex system is straightforward, but would require more intense computational effort. In higher dimensions, fluids can undergo phase transitions. In this respect, coarse-graining simplifies DFT modelling: by first treating the reference fluid with purely repulsive interactions, the possibility of liquid-gas coexistence and criticality is eliminated. The DFT of an attractive-repulsive fluid can be obtained by adding a simple mean-field term to the reference DFT, which provides a good approximation in many cases of practical interest (2). Of-course, hard-particle fluids can undergo freezing, and this possibility can be built into $F[\rho]$ by using trial functionals with singular terms. However in most liquid-state problems the temperature is sufficiently high that the system is not frozen. In these cases, the coarse-grained DFT can be sufficiently accurate, yielding, e.g., surface phase transitions during adsorption, even when the reference functional does not describe freezing (5).

A. Direct and inverse problems of statistical mechanics. The direct problem of equilibrium statistical mechanics in the DFT formulation, is to find the probability distribution function $\rho(\mathbf{r})$ over the positions of N interacting particles, moving in an external field $V(\mathbf{r})$, by minimising the *known* free energy functional $F[\rho] + \int \rho(\mathbf{r})V(\mathbf{r})d\mathbf{r}$, under the constraint $\int \rho(\mathbf{r})d\mathbf{r} = N$. Note that $F[\rho]$ is independent of $V(\mathbf{r})$. Choosing $V(\mathbf{r})$ to be singular can be used to describe the geometric confines of the system by assigning infinitely strong repulsive force to the walls, or even to restrict the motion of the particles to low-dimensional spatial manifolds. Thus, knowing $F[\rho]$ allows us in principle to compute the collective statistics of the system in any spatially confined setting, as well as in the bulk. Formally, we can cast the minimisation problem in terms of a Lagrangian $\Omega[\rho]$, introducing μ , the dual of ρ :

$$\Omega[\rho] = F[\rho] + \int \rho(\mathbf{r}) (V(\mathbf{r}) - \mu) d\mathbf{r}. \quad [1]$$

Because Ω can also be obtained directly from the system's Hamiltonian, by computing the grand-canonical partition function (6), we can get physically meaningful results after applying just the first part of the minimax principle, minimising Eq. (1) at a given μ . Fixing μ instead of N is equivalent to considering an open system, where N fluctuates around its average μ -dependent value $\langle N_\mu \rangle$. In this case, we say that the system is connected to a particle reservoir, held at chemical potential μ . In statistical physics, considering systems at fixed N is known as the canonical ensemble, whereas fixing μ instead is the grand-canonical ensemble. In the thermodynamic limit, both ensembles are equivalent, but systems with small N or $\langle N_\mu \rangle$ may exhibit significant differences when treated using different ensembles (7). The form of the DFT Eq. (1) is the same in both ensembles, the differences are subsumed by the definition and interpretation of $F[\rho]$. Traditionally, the grand-canonical ensemble is implied with classical DFT, however our proposed framework is able to infer both canonical and grand-canonical settings, based on the observed data.

The inverse problem of statistical mechanics can be formulated as finding an *unknown* $F[\rho]$, using M observations of the instantaneous coordinates of the system's particles. The data can be obtained using Monte-Carlo or molecular dynamics simulations in the relevant ensemble (6). Adopting a Bayesian paradigm, given the particle data, we compute a posterior distribution over all possible free energies consistent with the observed data. Our approach is markedly different from the traditional modelling approach which aims to construct a single tractable approximation for $F[\rho]$ which is only valid under idealised conditions. A similar philosophy was adopted in Ref. (8) to reconstruct the mean-field interparticle potential in graphene. In Ref. (9), the choice of free energy is formulated as a classification problem, and neural networks are used.

B. A Physically-consistent Free Energy Model. We can always express $F[\rho]$ as a sum of the ideal free energy and the excess-over-ideal term $F_{ex}[\rho]$:

$$F[\rho] = \beta^{-1} \int \rho(\mathbf{r}) (\ln \lambda^3 \rho(\mathbf{r}) - 1) d\mathbf{r} + F_{ex}[\rho], \quad [2]$$

where λ is the thermal wavelength, which includes the contribution from the Maxwell distribution of particle velocities and β is the inverse temperature. It is customary to set $\lambda = 1$, because changing λ produces only a shift of the chemical potential and it does not affect any thermodynamic or structural properties. In the grand-canonical ensemble, after $\rho(\mathbf{r})$ is obtained by minimising Eq. (1), the rest of the correlation-function hierarchy can be recovered by computing the inverses of the functional derivatives of $F_{ex}[\rho]$ at $\rho(\mathbf{r})$. Thus, DFT is indeed just a convenient formulation of statistical mechanics.

Interactions in a hard-particle fluid are purely repulsive, caused by volume exclusion and the fact that the particles have finite sizes and impenetrable cores. For such fluids, the most successful approximations for $F_{ex}[\rho]$ build on a physical insight, which we will also use as the basis for the physics-informed statistical inference of $F_{ex}[\rho]$. When particle interactions are pairwise and given by potential $\phi(r)$, $F_{ex}[\rho]$ can be expanded as a so-called Virial:

$$\beta F_{ex}[\rho] = -\frac{1}{2} \int \rho(\mathbf{r}_1) d\mathbf{r}_1 \int \rho(\mathbf{r}_2) f(\mathbf{r}_{12}) d\mathbf{r}_2 + \frac{1}{6} \int \rho(\mathbf{r}_1) d\mathbf{r}_1 \int \rho(\mathbf{r}_2) d\mathbf{r}_2 \int \rho(\mathbf{r}_3) f(\mathbf{r}_{12}) f(\mathbf{r}_{23}) f(\mathbf{r}_{13}) d\mathbf{r}_3 + \mathcal{O}(\rho^4), \quad [3]$$

where $\mathbf{r}_{ij} = |\mathbf{r}_i - \mathbf{r}_j|$ and $f(r) = \exp(-\phi(r)) - 1$ is the Mayer function. For hard-particles, the Mayer function is equal to -1 in the spatial regions where the particles overlap and zero otherwise. Thus, $f(r)$ can be expressed as a weighted sum of convolutions of the so-called geometric *fundamental measures* – window-functions $\{\omega_i(\mathbf{r})\}$, which characterize the shape of the particles in terms of volume, surface area, Gaussian and deviatoric curvatures (10). Using this fact, we can cast the low-density asymptote of Eq. (3) in terms of the weighted densities $n_i(\mathbf{r})$, given by the convolutions of $\rho(\mathbf{r})$ with each $\omega_i(\mathbf{r})$:

$$\beta F_{ex}[\rho] \underset{\rho \rightarrow 0}{\sim} - \int \sum_{i,j} n_i(\mathbf{r}) n_j(\mathbf{r}) d\mathbf{r}, \quad [4]$$

$$n_i(\mathbf{r}) = \omega_i * \rho \equiv \int \omega_i(\mathbf{r} + \mathbf{t}) \rho(\mathbf{t}) d\mathbf{t} \quad [5]$$

where the number of terms in the sum in Eq. (4) depends on the number of non-zero fundamental measures and is determined by the particle shape and fluid dimensionality. For example, the 3D molecule of a hard sphere fluid, where each particle is a sphere of radius R , can be described by five window-functions of \mathbf{r} (4): two scalar-valued functions $\Theta(R - |\mathbf{r}|)$, $\delta(R - |\mathbf{r}|)$ describing the volume and surface fundamental measures, and one vector-valued function $\mathbf{r}/|\mathbf{r}| \delta(R - |\mathbf{r}|)$ describing the mean curvature. Here $\Theta(x)$ is the Heaviside function and $\delta(x)$ is the Dirac delta-function. In the case of the 1D HR fluid with rods of width $2R$, $\mathbf{r} \equiv x$ and there are only two window-functions, corresponding to the volume and surface fundamental measures: $\omega_v(x) = \Theta(R - |x|)$ and $\omega_s(x) = \delta(R - |x|)/2$. According to Eq. (5), these give rise to the respective weighted densities $\eta(x)$, and $n_0(x)$:

$$\eta(x) = \int_{x-R}^{x+R} \rho(t) dt, \quad n_0(x) = \frac{\rho(x-R) + \rho(x+R)}{2}. \quad [6]$$

The fact that Eq. (4) is a local functional of $\{n_i\}$ prompts the physical intuition to approximate $F_{ex}[\rho]$ as a *local* functional of $\{n_i\}$, and forms the basis of our inference framework:

$$F_{ex}[\rho] = \beta^{-1} \int \Phi(n_1(\mathbf{r}), n_2(\mathbf{r}), \dots) d\mathbf{r}, \quad [7]$$

where $\Phi(\{n_i\}) \equiv \Phi(n_1(\mathbf{r}), n_2(\mathbf{r}), \dots)$ is a multivariate function of $\{n_i\}$. Notice that the 2nd and higher terms of Eq. (3) cannot be directly expressed as local functionals of the weighted densities. Under the ansatz Eq. (7), the construction of approximate $F_{ex}[\rho]$ essentially requires one to postulate an adequate $\Phi(\{n_i\})$, such that the resulting $F_{ex}[\rho]$ will extrapolate Eq. (4) to higher ρ . Such construction is not unique: observe that any function which integrates to zero can be added to $\Phi(\{n_i\})$ in Eq. (7). Over the years many sophisticated methods of increasing complexity have been proposed, employing matched asymptotics, dimensional analysis and dimensional cross-over. These gave rise to a plethora of approximate DFTs, collectively known as the Fundamental Measure Theory (FMT) (4). Yet, even in the case of simple hard sphere fluids, a universally acceptable approximate $F_{ex}[\rho]$ is elusive: some functionals fail to recover phenomenological thermodynamic equation of state of a hard-sphere fluid, others exhibit divergences in situations when the motion of the fluid particles is confined to low-dimensional manifolds, others still fail to adequately capture the freezing of hard spheres. Nevertheless, practical use of approximate hard sphere DFTs for computations (usually, as a reference part of a coarse-grained functional of an attractive-repulsive fluid, such as a Lennard-Jones fluid), typically involves a well-defined range of temperatures and pressures of interest. For such restricted well-defined regimes, one can in most cases select a satisfactory hard-sphere FMT approximation.

Thus, from a practical standpoint there is a clear need for a general method to obtain a computationally tractable approximate DFT functional, which would have well-defined limits of applicability given, e.g. by a range of fluid pressures or bulk densities of interest. In what follows, we borrow the most successful aspect of the best existing FMT approximations: the dependence on fundamental measures expressed by Eq. (7), and integrate this into a Bayesian statistical inference framework, permitting us to combine information from simulated particle trajectories with fundamental underpinning physical principles. As mentioned above, we consider the simplest case of a 1D fluid of HR on a line.

2. Bayesian inference of the grand-canonical density functional

A one-dimensional system of hard rods inside a pore of width L is sketched at the top of Fig. 1(a). When the fluid is held at the chemical potential μ , its collective behaviour, described by the grand-canonical ensemble, can be simulated yielding the expected number of particles $\langle N_\mu \rangle$ in the pore and a set of M instantaneous particle positions $\{y_i\}_{i=1}^M$. These form our fixed- μ training data set \mathcal{D}_μ :

$$\mathcal{D}_\mu = (\mu, \{y_i\}_{i=1}^M, \langle N_\mu \rangle). \quad [8]$$

Data generation is described in Appendix A. When M is sufficiently large, the histogram of $\{y_i\}_{i=1}^M$ should approximate the DFT density profile $\rho(x)$, which minimizes the Lagrangian in Eq. (1). We assume that $F_{ex}[\rho]$ is given by Eq. (7) with $\Phi(n_0, \eta)$ a function of two weighted densities given in Eq. (6). Thus, $\rho(x)$ solves the Euler-Lagrange, equation

$$\ln \rho(x) + \left(\omega_v * \frac{\partial \Phi}{\partial \eta(x)} + \omega_s * \frac{\partial \Phi}{\partial n_0(x)} \right) - \beta \mu = 0, \quad \text{subject to} \quad \int_{-L/2}^{L/2} \rho(x) dx = \langle N_\mu \rangle. \quad [9]$$

We adopt a straightforward and fairly general polynomial parametrisation of $\Phi(n_0, \eta)$ in terms of model parameters Q :

$$\Phi(n_0, \eta) \equiv \Phi(n_0, \eta | Q) = (a_{N_1} n_0(x)^{N_1} + a_{N_1-1} n_0(x)^{N_1-1} + a_0) (b_{N_2} \eta(x)^{N_2} + \dots b_0), \quad [10]$$

where $Q = (a_{N_1}, \dots, a_0, b_{N_2}, \dots, b_0)^T$ has $N_Q = N_1 + N_2 + 2$ elements. To avoid the equivalence between $\Phi(n_0, \eta | Q)$ and $\Phi(n_0, \eta | -Q)$, we constrain a_0 to be non-negative. During training, we will have to solve Eq. (9) numerically for a given Q , which is done using a Newton scheme. The most numerically stable way to discretize Eq. (6) for our purposes is with a simple linear interpolant, using trapezium rule for the quadratures in Eqs. (6) and (9). We want to find a posterior parameter distribution $P(Q)$, which induce two other distributions: one over free energy functionals $F[\rho | Q]$, via the term $\Phi(n_0, \eta | Q)$, and another one over the densities $\rho(x | Q)$, via Eq. (9). If one is required to characterise this distribution by a single value then one can obtain the expectation $\rho_E(x) = \int \rho(x | Q) dP(Q)$, or alternatively, the maximum a-posteriori estimate (MAP), $\rho_{\text{MAP}}(x) = \rho(x | \text{argmax}_Q P(Q))$.

As mentioned above, in the case of the hard-rod fluid in the grand-canonical ensemble, the exact free energy is given by $\Phi(n_0, \eta)$ is given by $\Phi_X(n_0, \eta) = -n_0 \log(1 - \eta)$ (3). This allows us to assess the quality of inference of the grand-canonical free energy functional by comparing $\rho(x | Q)$ against the exact distribution $\rho_{X|\mu}(x)$, which solves equation Eq. (9) with $\Phi = \Phi_X$. Note that since $\Phi(n_0, \eta)$ is not unique, we do not expect to retrieve exactly $\Phi_X(n_0, \eta)$.

A. Bayesian Inference Procedure. In the Bayesian paradigm, we choose prior distribution which characterise the behaviour of the coefficients Q in the absence of data. In this setting we choose a Gaussian prior with \bar{Q} (chosen at or near the origin) and a positive definite covariance matrix Σ_Q : $P_G(Q | \bar{Q}, \Sigma_Q) = (2\pi)^{-N_Q/2} (\det \Sigma_Q)^{-1/2} \exp(-\frac{1}{2}(Q - \bar{Q})^T \Sigma_Q^{-1} (Q - \bar{Q}))$. This prior distribution induces Φ to be a Gaussian random field in (n_0, η) with polynomial features. Clearly, not every configuration of Φ will yield an admissible free energy, and so, the prior variances on Q are chosen to constrain the components of Q to be sufficiently close to zero. The expression for likelihood follows from the physical interpretation of $\rho(x | Q)$ as the probability density of finding a particle near x :

$$P(\mathcal{D}_\mu | Q) = \prod_{i=1}^M \rho(y_i | Q). \quad [11]$$

The posterior distribution over Q is obtained from the Bayes rule, $P(Q | \mathcal{D}_\mu) \propto P_G(Q | \bar{Q}, \Sigma_Q) P(\mathcal{D}_\mu | Q)$, from which the predictive posterior distribution over $F[\rho]$ can be readily obtained. As $P(Q | \mathcal{D}_\mu)$ is not analytically tractable (indeed it is only known up to a normalising constant) and so approximate methods of inference must be considered. One such approach is to use a Markov Chain Monte Carlo (MCMC) approach, where a Markov chain is constructed whose samples are asymptotically distributed according to $P(Q | \mathcal{D}_\mu)$. To this end, we implement a Hamiltonian Monte-Carlo (HMC) algorithm to generate samples from the target distribution (11). This algorithm requires computing the gradient of the log-posterior $\nabla_Q \log P(Q)$ at every iteration of the chain, and therefore the gradient of log-likelihood in Eq. (11). The latter necessitates computing $\nabla_Q \rho$ – the Jacobian of the solution of Eq. (9) with respect to the parameter Q . Computing this gradient directly would require solving Eq. (9) $N_Q + 1$ times to evaluate $\nabla_Q \log P(Q)$ rendering it computationally infeasible even for moderate N_Q . Significant improvement can be achieved by using adjoint differentiation methods, which allow us to relate the numerical solution of Eq. (9) with its Jacobian with respect to Q via a simple linear system. The final expressions for log-posterior and its gradient used in HMC are given in Appendix B.

After tuning the HMC algorithm step-size and burn-in parameters to ensure that the output is stationary and sufficiently fast mixing, we generate samples from the HMC using a sufficiently long run of 4 independent chains. The empirical predictive distribution for $F[\rho]$ is then obtained from these samples analytically via Eqs. (10) and (7) and can be viewed as a distribution over free energies which is consistent with the observed simulation data. We illustrate this in Fig. 1, where we train the grand-canonical $F[\rho]$ at $\mu = 2$ and $L = 8$. Fig. 1(a) shows the histogram of the training data, the minimising densities $\rho(x)$ of the trained $F[\rho]$ (black), and the truth, given by the exactly known distribution $\rho_{X|\mu}(x)$ (red). We notice that we are able to approximate $\rho_{X|\mu}(x)$ with relatively few particle trajectories, attesting to the method's ability to combine essential physical assumptions with simulation data. Figs. 1 (b) and (c) show the predictions of the same $F[\rho]$ about the fluid in pores

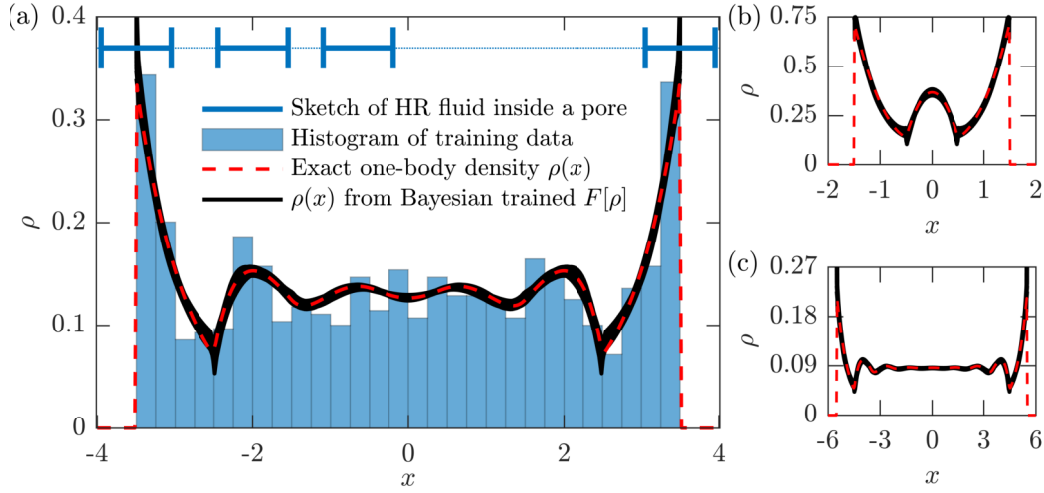


Fig. 1. Trained DFT functional for HR fluid at a fixed μ . (a) HR fluid, confined to a pore of width $L = 8$ and held at chemical potential $\mu = 2$, $\langle N_\mu \rangle = 4.6$. Particles of width $2R = 1$ interact via elastic collisions. $M = 1000$ simulated particle coordinates (histogrammed) were used to train $F[\rho]$ with $N_1 = N_2 = 5$ in Eq. (10). Black “curve” is the plot of 200 profiles $\rho(x)$, obtained from samples of the trained DFT functional. The “fuzziness” of the black curve characterises the uncertainty of the Bayesian scheme about $F[\rho]$. (b) and (c) show exact (dashed red) and sampled (black) $\rho(x)$ in pores with $L = 4$ and $L = 12$, obtained from the functional which was trained at $L = 8$. The agreement of plateaus of $\rho(x)$ in (c) demonstrates the retrieval of information about the bulk, contained in the configurations of the confined fluid.

with $L = 2$ and $L = 12$ (at the same $\mu = 2$), with superimposed $\rho_{X|\mu}(x)$. The thickness of the prediction curve indicates the standard deviation of the prediction at each point, capturing the local uncertainty which we note is largest around turning points of the DFT functional. This uncertainty can be reduced by increasing the training dataset size. For wide pores, the effects of the side walls are lost in the center, and the fluid behaviour is close to that of the bulk fluid. This is evidenced by the plateau of $\rho(x)$ in Fig. 1(c), which is correctly obtained and gives the density of the bulk HR fluid at our μ . This result is rather illuminating epistemologically: even though we were training on the data of a highly confined fluid inside a pore, we still managed to capture the physics of the bulk fluid, and obtained the correct equation of state.

B. A Gaussian random field model for chemical potential. A priori, one should not expect the model of Fig. 1 to generalise well beyond any value of μ not seen in the training dataset, which currently consists of a single value of μ . It is natural to consider extending the learning procedure in two ways: (i) by providing training data for multiple values of μ and (ii) extending the model to accommodate μ -dependence. At a first glance this may seem inconsistent with Eq. (2), where $F[\rho]$ does not explicitly depend on μ . However, we can view such inference model as a means of accommodating physical effects arising from the finiteness of the training data set and the finite dimensionality of Q . In the limit of infinitely large training datasets \mathcal{D} and N_Q , any built-in μ -dependence of Φ must disappear, as the true free energy functional is learned. On the other hand, when \mathcal{D} and N_Q are finite, it is worthwhile to expect the μ -dependent model to perform better, due to its higher flexibility and ability to interpolate/extrapolate to out-of-sample μ .

We model $\Phi(n_0, \eta | Q(\mu))$ by representing each element of Q as a degree M polynomial. Introducing an $N_Q \times (M + 1)$ matrix A of polynomial coefficients, we have

$$\Phi(n_0, \eta | \mu, \alpha) \equiv \Phi(n_0, \eta | Q(\mu | \alpha)), \quad Q(\mu | \alpha) = A (\mu^M, \mu^{M-1} \dots 1)^T, \quad [12]$$

where $\alpha = (\alpha_1, \dots, \alpha_{N_\alpha})^T$, $N_\alpha = N_Q(M + 1)$, is the (row-wise) flattened matrix A . The training data set \mathcal{D} and the likelihood function for this extended model become:

$$\mathcal{D} = \{\mathcal{D}_{\mu_n}\}_{n=1}^K \equiv \left\{ \left(\mu_n, \{y_{i|n}\}_{i=1}^{M_n}, \langle N_n \rangle \right) \right\}_{n=1}^K, \quad [13]$$

$$P(\mathcal{D} | \alpha) = \prod_{n=1}^K \prod_{i=1}^{M_n} \rho(y_{i|n} | \mu_n, \alpha), \quad [14]$$

where $M_n \equiv M_{\mu_n}$, $y_{i|n}$ is the i -th simulated particle coordinate at μ_n , $\langle N_n \rangle \equiv \langle N_{\mu_n} \rangle$, and $\rho(y_{i|n} | \mu_n, \alpha)$ is the solution of Eq. (9) with Φ given by Eqs. (10) and (12), at $\mu = \mu_n$. The joint Gaussian prior on the coefficients Q and α induces a Gaussian random field prior on the space of functions Φ of the variables n_0, η, μ .

As before, Eqs. (12)–(14) define a posterior distribution for Q and α given observed trajectory data, from which we may infer $F[\rho]$. This allows us to characterise the fluid for a broad range of μ , including very dilute and highly structured fluid configurations, using the same functional. As an illustration, consider the training dataset with $K = 8$ integer μ -points, $\mu = -2 \dots 5$, and $M_n = 10^4$ particle coordinates for each μ -point, drawn from a grand-canonical simulation of hard-rods fluid in a pore of width $L = 8$. We use it to train two functionals: a μ -independent one with $M = 0$ and a linear one with $M = 1$ in Eq. (12), both trained for $N_1 = 3$ and $N_2 = 8$ in Eq. (10). The results are represented in Fig. 2 in terms of the density profiles

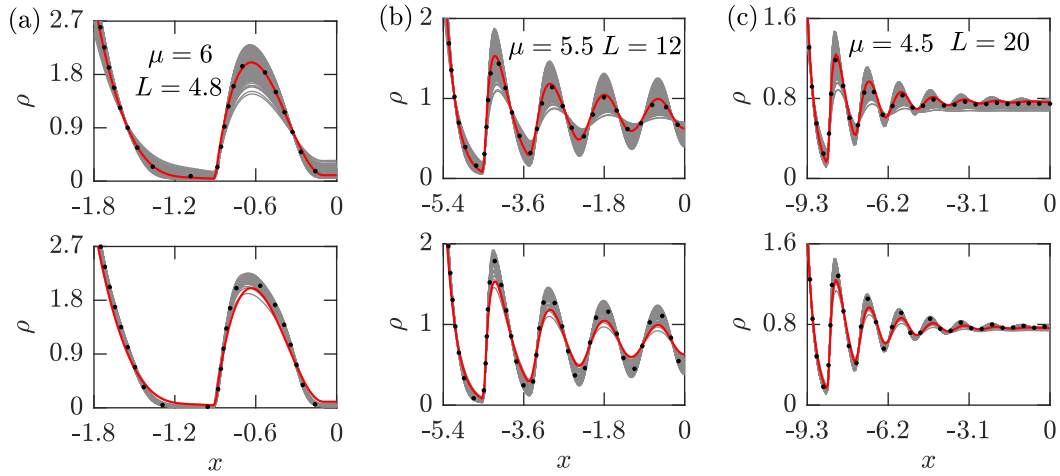


Fig. 2. Illustration of two trained functionals, which describe the fluid at different μ as given in Eqs. (12)–(14) with $N_1 = 3$ and $N_2 = 8$, trained at $K = 8$ integer values of $\mu = -2, \dots, 5$, with $M_n = 10^4$ particle coordinates for each μ . Plotted density profiles minimise Eq. (1) at the given μ and L . In (a)–(c), the top and bottom panels correspond to models with $M = 0$ and $M = 1$ in Eq. (12). Due to symmetry, the profiles are shown at $-L/2 \leq x \leq 0$. Posterior is shown by 400 uncorrelated samples (grey). The MAP estimate (black dots) lies close to the truth, $\rho_{X|\mu}(x)$ (red). Notice that uncertainty is less for $M = 1$, but MAP estimates at $M = 0$ in (a) and (b) show more agreement with $\rho_{X|\mu}(x)$ than at $M = 0$, and this is reversed in (c) [particularly noticeable near the pore centre in (c)]. This is an example of possible over-fitting in (a) and (b).

minimising Eq. (1) in a variety of pores and chemical potentials, chosen outside of the training dataset. The top and bottom plots in (a)–(c) correspond to μ -independent model, and linear μ -model, respectively. The point estimates (dotted) correspond to MAP, and the uncertainty of the inferred $F[\rho]$ is illustrated by plotting 400 uncorrelated samples from the posterior (grey). The exact $\rho_{X|\mu}(x)$ is plotted in red and shows remarkable agreement with the trained functional, particularly with MAP point estimate.

In accordance with Eq. (1), and as we already saw in Fig. 1, L does not matter, and $F[\rho]$, trained at some fixed L , describes the fluid well at any other L , even capturing bulk fluid density at large L [Figs. 1(c) and 2(c)]. A more interesting behaviour of the inferred $F[\rho]$ concerns μ -points outside of the training set. First we note that μ -dependent model shows significantly more confidence in its prediction than the μ -independent one. Indeed, the predictive posterior distribution forms a narrow band around the MAP estimator. By comparison, the posterior of the μ -independent model is more diffuse, demonstrating much more spread around the MAP estimator. The second observation is more subtle and concerns the difference between the two possible options for μ : either the chosen μ interpolates the training set [Fig. 2(c)] or extrapolates from it [Fig. 2 (a) and (b)]. We find that when μ extrapolates the training dataset, μ -independent model gives slightly better MAP estimates than the μ -independent model, even though the latter has less uncertainty. This is reversed for interpolation of the μ -dataset, where the linear model yields a better MAP estimate [as can be noticed from a close at the pore center in Fig. 2(c)]. The fact that the μ -dependent model has less uncertainty and is more accurate during interpolation can be attributed to its higher flexibility in fitting the dependencies. At the same time, the breakdown of the more complex model during extrapolation suggests there is over-fitting: the actual Φ is independent of μ , so imposing artificial μ -dependence allows us to fit the training data better, but sacrifices generalisation.

3. Inferring the canonical functional

So far we have been considering open systems, where the number of particles fluctuates around a mean $\langle N_\mu \rangle$, which is determined by the chemical potential. The hard-rods DFT is known exactly in this case, and we used this fact to simplify the benchmarking of our inferred $F[\rho]$ against the truth, given by $\rho_{X|\mu}(x)$. However, there are numerous important problems where one requires the DFT of a system with a fixed number of particles. For example, standard treatments of collective dynamics of out-of-equilibrium many-body systems lead to a Fokker-Plank equation for the time-dependent one-body density, which contains a free energy functional $F_N[\rho]$ of the system with a fixed number of particles N . For small systems, fluctuations of N become significant and important differences may arise between the ensembles (7) and Fig. 3. Furthermore, analytic attempts to derive $F_N[\rho]$ are scarce due to theoretical difficulties, and existing approximations are extremely challenging computationally, containing systems of coupled integral equations (12). Naturally, we are interested in benchmarking our inference methodology against this important case and trying to infer a reliable approximate $F_N[\rho]$ from particle data.

We can simulate N hard rod particles in a pore by removing the random particle insertion/deletion steps of the grand-canonical simulation, as described in Appendix A. In the canonical ensemble the direct problem discussed in Sec. A formally looks the same: We need to minimise Eq. (1), with $F[\rho] \equiv F_N[\rho]$. There is, however, one important distinction. In the canonical ensemble knowing the system's partition function is equivalent to knowing the minimised $F_N[\rho]$ and not $\Omega[\rho]$. As a result, $F_N[\rho]$ is a function of N , and $\Omega[\rho]$ is simply a Lagrangian of the constrained minimisation problem for $F_N[\rho]$. Additionally, μ is no longer a thermodynamic field, but simply the Lagrange multiplier. With this understanding, we proceed with the inference

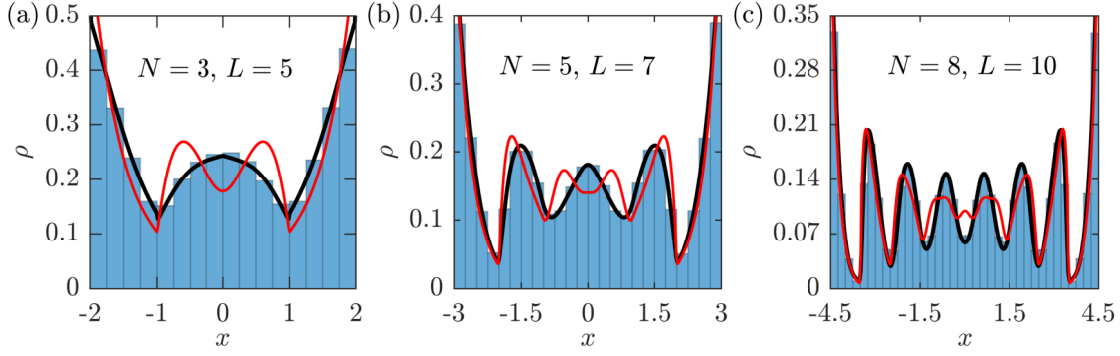


Fig. 3. Out-of-sample performance of the trained canonical-ensemble free energy functional $F_N[\rho]$. At each given N we trained the model $F_N[\rho]$ with $N_1 = N_2 = 4$ in Eq. (10) on 10^4 particle coordinates in each of $K = 6$ pores of varying width (not including the width shown). (a)–(c) show $\rho(x)$ minimising the respective $F_N[\rho]$ at posterior maximum (black), the exact grand-canonical $\rho_{X|\mu}(x)$ (red), computed at $\langle N_\mu \rangle = N$, and the histogram of particle coordinates. Notice the excellent agreement of the trained canonical $F_N[\rho]$ with the data, unlike its exact grand-canonical counterpart.

process as expressed in Eqs. (9) and (10) with $\langle N_\mu \rangle \equiv N$ on a dataset \mathcal{D}_N of canonical particle trajectories in K different pores:

$$\mathcal{D}_N = \{L_n, \{(y_1, \dots, y_N)\}_{i=1}^{M_n}\}_{n=1}^K. \quad [15]$$

In Fig. 3 we plot the result of the inference process for three small systems, where the canonical and grand-canonical ensembles give different results. For each L in (a)–(c) we trained $F_N[\rho]$ on 6 equi-spaced L_n , chosen between $L - 2$ and $L + 2$ with a step of 0.8, so that L shown is not in the training data set. We used $M_n = 10^4$ particle coordinates in each pore. Black curves show the MAP estimates of the posterior over $F_N[\rho]$, with the truth given in terms of the histogram of the particle coordinates. Notice an excellent agreement of the trained $F_N[\rho]$ with the histograms. To highlight the difference with the grand-canonical ensemble, we superimpose the exact grand-canonical $\rho_{X|\mu}(x)$, computed at such μ that $\langle N_\mu \rangle = N$. The difference between the ensembles is highest in the pore centres, where the exact grand-canonical functional wrongly predicts local minima of $\rho(x)$ in (a) and (b), and a local maximum in (c). Notice that as the system size increases, the difference between the ensembles diminishes, attesting to the fact that the limit $\mu \rightarrow \infty$ is equivalent to $2R\langle N_\mu \rangle \rightarrow L$ and both ensembles agree in this limiting case.

4. Data efficiency

In this section we assess the data efficiency and accuracy of the proposed physics-informed inference method in comparison to a baseline black-box distributional model. To this end we consider the following mixture model of Gaussian RBFs:

$$\rho(x | \mu) = \sum_{i=1}^{N_f} \alpha_i(\mu) \exp\left(-\frac{(x - p_i)^2}{w_i^2(\mu)}\right), \quad [16]$$

where $\alpha_i(\mu) \geq 0$ for all i and $\sum_j \alpha_j(\mu) = 1$, and $\{f(x | \theta_i)\}$ is a density on \mathbb{R} parametrised by θ_i . For generality, we can assume μ -dependence of the free parameters in Eq. (16). The RBF means p_i are fixed to be equispaced inside the computational domain. As before, we consider a fixed- μ and a variable- μ setting. The likelihoods of the former and the latter are given in Eqs. 11 and 14. We set up a Bayesian inference of Eq. (16). For the fixed μ setting, we place a Gaussian prior on w_i and a rectified prior distribution with mean 1 and variance 0.1 for the α_i , so that they are constrained to be non-negative. For variable- μ setting, we treat w_i as quadratic polynomial in μ , and α_i as the exponentiated quadratic polynomial in μ . We then place Gaussian priors with zero means and variances 0.1 on the polynomial coefficients.

Figs. 4 (a) and (b) provide a comparison at a fixed μ . Fig. 4(a) shows the MAP estimates obtained in the low training data regime. The physics-informed model performs very well here, coinciding with $\rho_{X|\mu}(x)$ in every feature. For this reason, we did not plot $\rho_{X|\mu}(x)$ in Fig. 4(a). The behaviour of the statistical RBF model is comparatively weaker. The RBF distribution is smooth, due to the smoothness of the underlying functional basis. Still, the training dataset is clearly not large enough to give a good approximation to $\rho_{X|\mu}(x)$. Particularly noticeable is the absence of symmetry. Increasing the training dataset improves the quality of the statistical model. We can quantify this in terms of the energy distance ΔE between $\rho_{X|\mu}(x)$ and the MAP-estimate $\rho(x)$ (13). The convergence of the physics-informed and brute-force models is shown in Fig. 4(b) as a function of the dataset size. Both vanish at large training data sets. Notice that the physics-informed model is at least an order of magnitude closer to the ground truth the statistical model at the same dataset size.

In Fig. 4(c) we compare the physics-informed model against the RBF statistical model in a high training data regime. Again, the physics-informed model performs well and is indistinguishable from $\rho_{X|\mu}(x)$. The RBF model clearly captures the essential features of $\rho_{X|\mu}(x)$ here. The noticeable disagreement signals that a bigger basis is required. Additionally we point out that the generalisation of the RBF model to μ far outside the training set is quite poor: a very dense training mesh covering the range of μ of interest is required to obtain the agreement shown in Fig. 4(c). We also obviously do not expect the statistical

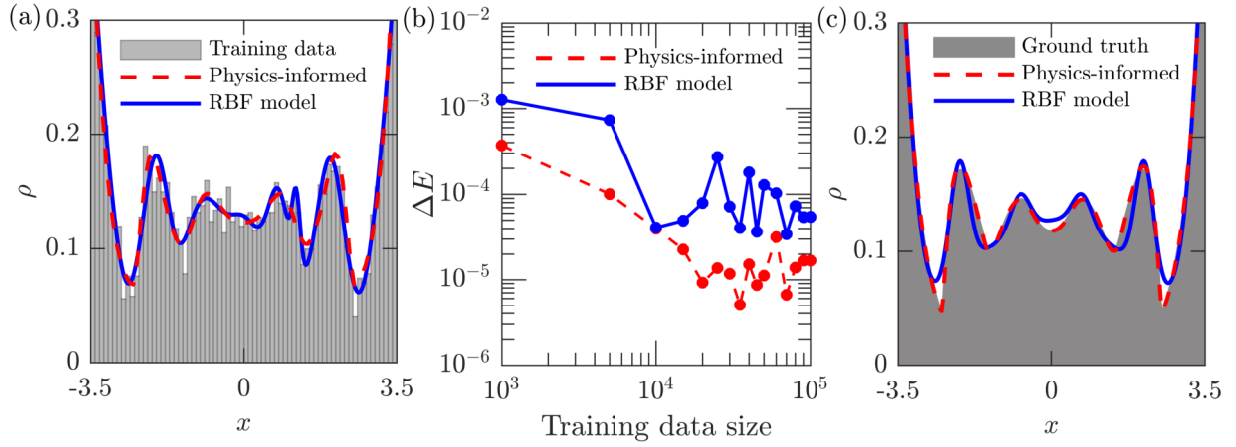


Fig. 4. Illustration of the data efficiency and flexibility of the physics-informed model. In (a)–(c), the physics-informed model has $N_1 = N_2 = 6$, $\mu = 3$, $L = 8$. (a) MAP-estimates at fixed- μ : physics-informed (red dashed) model is visually indistinguishable from the ground truth, given by $\rho_{X|\mu}(x)$ (not plotted); RBF model with $N_f = 21$ (blue). Both models were trained on the dataset of $M = 5 \times 10^3$ particle coordinates (plotted as a histogram). (b) Energy distance of models in (a) from $\rho_{X|\mu}(x)$ as a function of the training data size M . (c) Variable- μ physics-informed (red) and RBF model with $N_f = 10$ (blue) are both trained on $\mu = 2.7, 2.8, 2.9, 3.1, 3.2$ and 3.3 , with $M_i = 3 \times 10^4$; the ground truth is shown in grey.

model to generalize to different L values, unlike the physics informed model. The dependence on L must be explicitly built into Eq. (16), and then even larger datasets would be needed for training. This will further increase the comparative cost of the statistical brute-force approach to several orders of magnitude above the physics-informed approach.

5. Conclusion

We presented an inference methodology for finding the distributional model of the free energy of a many-body system using simulated particle trajectories. The broader scope of this work is that by coarse-graining interactions in realistic many-body systems, such as fluids and active matter, it is possible to systematically obtain the corresponding terms of the free energy functional of the system. We considered the prototypical case of a one-dimensional fluid, which is a natural first step for physics-informed inference in classical many-body systems. The generalisation of our method to higher dimensions is conceptually straightforward, and can be implemented by considering functionals of the general form $\Phi(\{n_i\})$. However, special care should be taken to properly train the inference model in regions, where the system undergoes phase transitions. In particular, the parametric form of $\Phi(\{n_i\})$ should allow for singular behaviour.

Epistemologically, the proposed method corresponds to the systematic propagation of uncertainty through all logical levels of modelling. The subjectivity is quantified by the choice of the prior distribution. This can be contrasted with the traditional approaches to analytic derivations, which require maintaining some sort of analytic tractability during model development. In this respect, the developed inference method allows us to scale up model complexity. By prioritising data above simplifying assumptions, we maintain a direct connection with experiment, while offering an epistemologically different way to approach model development by numerically sampling the distributional model of a highly flexible underlying approximant.

ACKNOWLEDGMENTS. PY was supported by Wave 1 of The UKRI Strategic Priorities Fund under the EPSRC Grant EP/T001569/1, particularly the “Digital Twins for Complex Engineering Systems” theme within that grant, and The Alan Turing Institute. ABD was supported by the Loyds Register Foundation Programme on Data Centric Engineering and by The Alan Turing Institute under the EPSRC grant [EP/N510129/1]. PY thanks Carlos Rasón and Yuri Martínez-Ratón for an illuminating discussion.

Appendix A

Grand-canonical algorithm to produce a set of particle coordinates of a HR fluid inside a pore of width L at chemical potential μ is given in Table 1. The canonical algorithm for a fixed number of $N = N_i$ particles inside the same pore is given by repeating only steps 1-2.

Table 1. Algorithmic view of the grand-canonical ensemble of hard rods of radius R in a pore of width L , at chemical potential μ

- 0 Starting with a random integer $1 \leq N_0 \leq L/2R$ (initial number of particles in the pore), do 1–3 in a loop over $i = 0, 1, \dots$
- 1 Randomly draw $N_i + 1$ non-negative real numbers with the sum equal to $(L - 2RN_i)$.
These give lengths of $N_i - 1$ particle-particle gaps and 2 particle-wall gaps;
- 2 Compute coordinates $\mathcal{Y}_i = (y_1, \dots, y_{N_i})$ of N_i particles from the gaps of step 1;
- 3 Obtain the new number of particles $N_{i+1} \in \{N_i - 1, N_i, N_i + 1\}$ by attempting particle insertion/deletion with probabilities $P_{\text{del}}/P_{\text{ins}}$;
 $P_{\text{del}} = \{N_i \exp(-\mu)/(L/2R) \text{ if } N_i > 1 \text{ and } 0 \text{ otherwise}\}$, $P_{\text{ins}} = \{(L/2R) \exp(\mu)/(N_i + 1) \text{ if } N_i + 1 < L/2R \text{ and } 0 \text{ otherwise}\}$

To build a set of M particle coordinates in the grand-canonical ensemble, we run the steps 1–3 for approximately ML/R iterations, to obtain the cumulative flattened data set $(\mathcal{Y}_1, \mathcal{Y}_2, \dots)$. Then we uniformly thin it to reduce correlations between y_i , keeping M particle

coordinates $\{y_i\}_{i=1}^M$, and compute the expected number of particles in the pore:

$$\langle N_\mu \rangle = \frac{1}{M_\mu} \sum_{i=1}^{M_\mu} N_i. \quad [17]$$

Appendix B

At a fixed μ , the HMC sampler for posterior $P(Q)$ is implemented with the following expressions for log-posterior and its gradient:

$$\log P(Q) = \log P_G(Q | \bar{Q}, \Sigma_Q) + \sum_{i=1}^{M_\mu} \log \frac{\rho(y_i | Q)}{\langle N_\mu \rangle}, \quad [18]$$

$$\nabla_Q \log P(Q) = -\Sigma_Q^{-1} (Q - \bar{Q}) + \sum_{i=1}^{M_\mu} \nabla_Q \rho(x) \Big|_{x=y_i} \frac{1}{\rho(y_i | Q)}. \quad [19]$$

1. JF Lutsko, Recent Developments in Classical Density Functional Theory in *Adv. Chem. Phys.* (John Wiley & Sons), p. 1 (2010).
2. J Wu, Z Li, Density-Functional Theory for Complex Fluids. *Annu. Rev. Phys. Chem.* **58**, 85 (2007).
3. JK Percus, Equilibrium State of a Classical Fluid of Hard Rods in an External Field. *J. Stat. Phys.* **15**, 505 (1976).
4. P Tarazona, JA Cuesta, Y Martinez-Raton, Density Functional Theories of Hard Particle Systems in *Theory and Simulations of Hard-Sphere Fluids and Related Systems. Lecture Notes in Physics* 753, ed. A Mulero. (Springer, Berlin Heidelberg), p. 251 (2008).
5. P Yatsyshin, AO Parry, S Kalliadasis, Complete Prewetting. *J. Phys.: Condens. Matter* **28**, 275001 (2016).
6. MP Allen, DJ Tildesley, *Computer Simulations of Liquids*. (Oxford Science Publications), (1989).
7. JL Lebowitz, JK Percus, L Verlet, Ensemble Dependence of Fluctuations with Application to Machine Computation. *Phys. Rev.* **153**, 250 (1967).
8. A Yousefzadi Nobakht, et al., Reconstruction of effective potential from statistical analysis of dynamic trajectories. *AIP Adv.* **10**, 065034 (2020).
9. SC Lin, G Martius, M Oettel, Analytical classical density functionals from an equation learning network. *The J. Chem. Phys.* **152**, 021102 (2020).
10. R Wittmann, M Marechal, K Mecke, Fundamental measure theory for smectic phases: Scaling behavior and higher order terms. *The J. Chem. Phys.* **141**, 064103 (2014).
11. S Brooks, *Handbook of Markov chain Monte Carlo*. (Taylor & Francis, Boca Raton), (2011) OCLC: 753969788.
12. J White, A Gonzalez, F Roman, S Velasco, Density-Functional Theory of Inhomogeneous Fluids in the Canonical Ensemble. *Phys. Rev. Lett.* **84**, 1220–1223 (2000).
13. GJ Székely, ML Rizzo, Energy statistics: A class of statistics based on distances. *J. Stat. Plan. Inference* **143**, 1249–1272 (2013).